Role of the S4 Segment in a Voltage-dependent Calcium-sensitive Potassium (h*Slo*) Channel*

Laín Díaz‡, Pratap Meera§, Julio Amigo‡, Enrico Stefani§¶‖, Osvaldo Alvarez‡, Ligia Toro§** ‡‡ §§, and Ramon Latorre‡§¶ ¶¶**

*From the ‡Departamento de Biología, Facultad de Ciencias, Universidad de Chile and ¶Centro de Estudios Científicos de Santiago Casilla 16443, Santiago 9, Chile, and the Departments of §Anesthesiology, ‖Physiology, and ‡‡Molecular and Medical Pharmacology and the **Brain Research Institute, UCLA, Los Angeles, California 90095-1778*

We investigated the role of individual charged residues of the S4 region of a MaxiK channel (h*Slo*) in channel gating. We measured macroscopic currents induced by wild type (WT) and point mutants of h*Slo* in inside-out membrane patches of *Xenopus laevis* oocytes. Of all the residues tested, only neutralizations of Arg-210 and Arg-213 were associated with a reduction in the number of gating charges as determined using the limiting slope method. Channel activation in WT and mutant channels was interpreted using an allosteric model. Mutations R207Q, R207E, and R210N facilitated channel opening in the absence of Ca^{2+}; however, this facilitation was not observed in the channels Ca^{2+}-bound state. Mutation R213Q behaved similarly to the WT channel in the absence of Ca^{2+}, but Ca^{2+} was unable to stabilize the open state to the same extent as it does in the WT. Mutations R207Q, R207E, R210N, and R213Q reduced the coupling between Ca^{2+} binding and channel opening when compared with the WT. Mutations L204R, L204H, Q216R, E219Q, and E219K in the S4 domain showed a similar phenotype to the WT channel. We conclude that the S4 region in the h*Slo* channel is part of the voltage sensor and that only two charged amino acid residues in this region (Arg-210 and Arg-213) contribute to the gating valence of the channel.

Large conductance Ca^{2+}-dependent K^+ (MaxiK)[1] channels are sensitive to both the transmembrane potential and to the internal calcium concentration ($[Ca^{2+}]$). The probability of finding these channels in the open state increases with positive potentials or with increments of $[Ca^{2+}]$ (1, 2). MaxiK channels share many features with voltage-dependent Na^+, Ca^{2+}, and K^+ channels of the S4 superfamily (3). One of the most remarkable features is that MaxiK channels also contain the S4 common motif, a structure with a repeated triple sequence of one positively charged amino acid (arginine or lysine) plus two hydrophobic amino acids (4–13). Because it is highly charged, the S4 region has been suggested to serve as the voltage sensor (14–16). In voltage-dependent K^+ channels the evidence supporting this view is becoming overwhelming (17–25).

We have recently shown that MaxiK channels possess an intrinsic voltage sensor whose rearrangement triggered by voltage induces measurable gating currents (27). Both charge movement and pore opening are facilitated by $[Ca^{2+}] > 100$ nM (26, 27). We examine here the contribution of individual charged residues of the S4 region to the voltage dependence and Ca^{2+} sensitivity of a cloned human MaxiK channel, h*Slo,* using site-directed mutagenesis. We conclude that: (*a*) the S4 region in the h*Slo* channel is part of the voltage sensor; (*b*) for all the S4 mutants tested only two charged amino acid residues appear to modify the limiting slope of the probability of opening *versus* voltage curves; (*c*) for all S4 mutants, there is a $[Ca^{2+}]$ region ($\leq$100 nM) in which channel activity becomes independent of the $[Ca^{2+}]$. We performed an analysis of the half-activation voltages-$[Ca^{2+}]$ data for the WT h*Slo* and the S4 mutant channels using a gating scheme drawn from the Monod-Wyman-Changeaux (MWC) model for allosteric proteins (28). The model describes the data reasonably well and indicates that shifts in the P_o-V curves along the voltage axis induced by the mutations in the S4 domain are due to stabilization of the open configuration and to a decrease in the coupling between Ca^{2+} binding and channel opening.

MATERIALS AND METHODS

Clones, Mutagenesis, and in Vitro Transcription—All experiments were performed on the high conductance, calcium-dependent K^+ channel, h*Slo*, cloned from human myometrium (11). Channels were expressed from h*Slo* cDNAs starting from the third Kozak consensus sequence (M3). Constructs contained as 5′-untranslated region, 86 base pairs upstream M3 of h*Slo* or 223 base pairs of 5′-untranslated region from *Shaker* H4. S4 mutations were carried out on the latter version that also contained a poly(A) tail at the 3′-end and results in a higher level of expression (27).

Site-directed mutagenesis was performed with the polymerase chain reaction, based on the four-primer strategy (29, 30). After DNA amplification, sequencing checked the presence of mutations.

Wild type and S4 mutant RNAs of h*Slo* were *in vitro* transcribed using mMessage mMachine kit (Ambion Inc., Austin TX). The protocol used to isolate *Xenopus laevis* oocytes received institutional approval and followed NIH guidelines. Oocytes (stage V-VI) were treated with collagenase (≈450 units/ml, 60–90 min. at room temperature) in a Ca^{2+}-free medium (OR-2 (mM): NaCl 82.5, KCl 2.5, $MgCl_2$ 1, HEPES 5, pH 7.6) and then washed five times with ND-96 (in mM: NaCl 96, KCl 2, $MgCl_2$ 1, $CaCl_2$ 1.8, HEPES 5, pH 7.6). Twenty-four hours later they were microinjected with 50 nl of 0.01–0.5 μg/μl mRNA in water. Oocytes were maintained at 18 °C in ND-96 supplemented with gentamycin (50 μg/ml).

Electrophysiological Recordings—After the manual removal of the vitellin membrane, macroscopic currents were evoked in membrane patches in the inside-out configuration. Current records were obtained

* This work was supported in part by Chilean Grants FNI 1970739 (to R. L.), FNI 2950028 and 4960005 (to L. D.), by grants from Catedra Presidencial and a group of Chilean companies (CODELCO, CMPC, CGE, Minera Escondida, Minera Collahuasi, NOVAGAS, Business Design Ass., and XEROX Chile) (to R. L.), and by National Institutes of Health Grants HL54970 (to L. T.) and GM52203 (to E. S.). The costs of publication of this article were defrayed in part by the payment of page charges. This article must therefore be hereby marked "*advertisement*" in accordance with 18 U.S.C. Section 1734 solely to indicate this fact.

§§ Established Investigator of the American Heart Association.

¶¶ To whom correspondence should be addressed: Centro de Estudios Científicos de Santiago, Casilla 16443, Las Condes, Santiago 9, Chile. Tel.: 562-233-8342; Fax: 562-233-8336; E-mail: ramon@cecs.cl.

[1] The abbreviations used are: MaxiK, large conductance Ca^{2+}-dependent K^+ channels; h*Slo,* cloned human MaxiK channel; WT, wild type; $[Ca^{2+}]$, calcium concentration; P_o, probability of opening; G, conductance; $V_{½}$, half-activation potential; LSM, limiting slope method; MWC, Monod-Wyman-Changeaux.

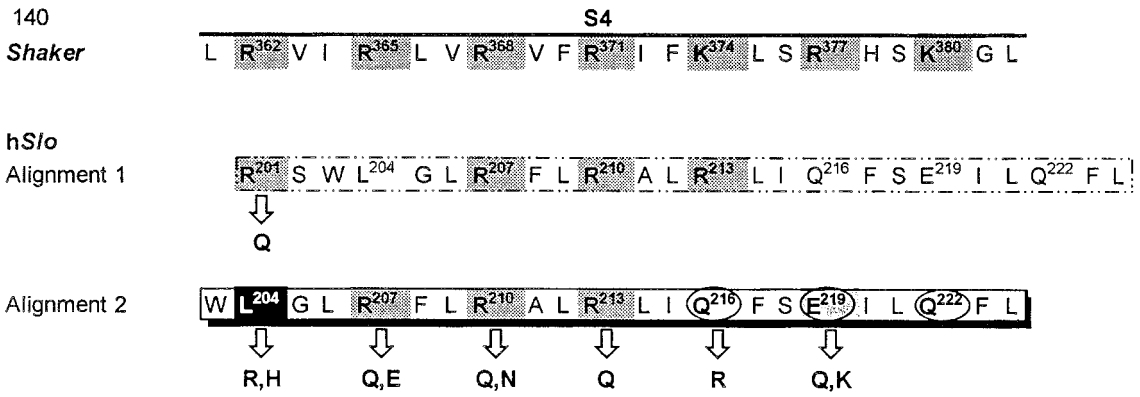

FIG. 1. **Primary structure alignment of h*Slo* and *Shaker* S4 segments.** Alignment 1 was obtained from a multiple sequence alignment with other voltage gated K^+ channels (34), but the S4 segment includes residues R362 in *Shaker* and R201 of h*Slo*. Alignment 2 was obtained from a multiple sequence alignment with voltage gated K, Ca, and Na channels, using 400 N-terminal amino acids from h*Slo* (34). The Pileup program of the Genetics Computer Group software and default settings were used. *Gray boxes,* conserved positively charged residues. Also highlighted are the polar (*ellipse*), the negative (*gray ellipse*), and the hydrophobic (*black box*) residues of h*Slo* that in *Shaker* are positively charged. *Arrows* mark the mutations studied.

2–6 days after injection of the oocytes. The pipettes had 1–2 megohm resistances, and no series resistance compensation was used. The error due to uncompensated series resistance was never greater than ~5 mV. Pipettes were filled with (mM): 110 potassium methanesulfonate, 10 HEPES, 2 $MgCl_2$, pH 7.0. The free $[Ca^{2+}]$ in the bath solution, which faces the intracellular side of the membrane in the inside-out patch configuration, was buffered with Ca^{2+} chelators and calculated with the software CHELATOR (31). From 10 nM to 3 mM free Ca^{2+}, all of the solutions had (mM): 110 potassium methanesulfonate, 10 HEPES, and 5 HEDTA, pH 7.0. The desired free $[Ca^{2+}]$ was set adding concentrated $CaCl_2$ to this base solution. Free $[Ca^{2+}]$ was measured with a Ca^{2+} electrode (World Precision Instruments, Sarasota, FL). Solutions with $[Ca^{2+}]$ less than 10 nM were obtained by replacing the corresponding amount of methanesulfonate with 10 mM HEDTA (1.5 nM free Ca^{2+}), 10 mM EGTA (363 pM free Ca^{2+}), 70 mM EGTA (52 pM free Ca^{2+}), 10 mM EDTA (55 pM free Ca^{2+}), or 70 mM EDTA (8 pM free Ca^{2+}).

Acquisition and Analysis—The current signal was digitized to a frequency equal to 5 times the filter cutoff frequency. The acquisition and basic analysis of the data were performed with pClamp 6.0 software (Axon Instrument, Inc.). To obtain the maximum conductance, G_{max}, membrane patches were stimulated with rectangular voltage pulses and steady-state I-V curves were constructed. Conductance (G) *versus* voltage relationships were obtained from the relation $G = I/(V - E_K)$ where I is the measured K^+ current and E_K is the K^+ equilibrium potential. The data were well described by a Boltzmann function of the form

$$P_o = G/G_{max} = [1 + \exp(-z_{eq}F(V - V_{1/2})/RT)]^{-1} \qquad \text{(Eq. 1)}$$

where P_o is the probability of channel opening, $V_{1/2}$ is the voltage at which $P_o = 0.5$; z_{eq} is the equivalent gating charge associated with the closed to open transitions, and R, T, and F have their usual meanings. G_{max}, $V_{1/2}$, and z_{eq} were obtained using a non-linear curve fitting procedure. Maximum conductance was an adjustable parameter in those patches in which artifacts introduced by fast Ca^{2+} block and non-linearity of the instantaneous current-voltage relation (32, 33) were minimal. This G_{max} was used to fit $V_{1/2}$ and z_{eq} at those $[Ca^{2+}]$ where the determination of G_{max} was unreliable. The validity of this method of determining G_{max} was checked using tail current measurements (33).

RESULTS

Point Mutations in the S4 Segment of hSlo—We have tested a series of S4 mutants in a quest to find the role of this transmembrane segment in h*Slo* channels. Fig. 1 shows two possible alignments for h*Slo* S4 segment. Alignment 2 predicts an h*Slo* S4 segment with only 3 positive residues (arginines) at 207, 210, and 213, compared with 7 in *Shaker* K^+ channels. We have substituted these positively charged residues of S4 by either neutral (glutamine or asparagine) or negative (glutamate) residues. Other positions, that are basic amino acids in *Shaker*, are hydrophobic (Leu-204), polar (Gln-216, Gln-222), or acidic (Glu-219) in h*Slo*. In these positions, the following point mutations were performed: L204R, L204H, Q216R, E219Q and E219K. In alignment 1 (34), residue Arg-201 could also form part of h*Slo* S4 segment. We have neutralized this residue to glutamine (R201Q). In all the cases tested, mutations in the S4 segment of h*Slo* produced functional channels.

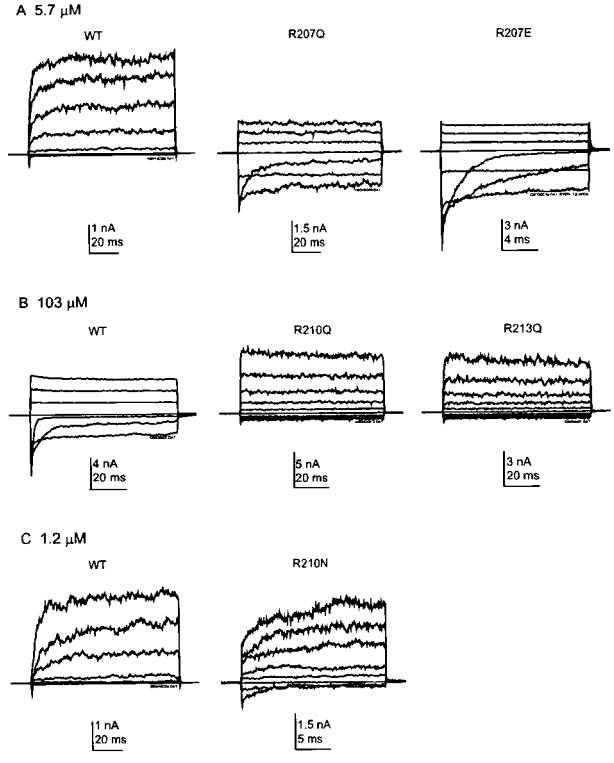

FIG. 2. **Macroscopic currents for wild type h*Slo* and S4 mutant channels.** Currents were recorded from inside-out macropatches. Holding voltage was 0 mV. *A*, internal $[Ca^{2+}]$ was 5.7 μM. Currents were elicited by voltage steps to −100, −50 and from 0 to 100 mV with increments of 20 mV for WT h*Slo* channels; and by voltage steps to −200, −150, −50 and from 0 to 60 mV in increments of 20 mV for R207Q and R207E mutants. For R207E an additional current trace elicited by a voltage step to −250 mV is shown. *B*, internal $[Ca^{2+}]$ was 103 μM. WT currents were induced by voltage steps to −140, −80, −50 and from 0 to 60 mV in increments of 20 mV, and R210Q and R213Q currents were induced by voltage steps from −100 to −25, in increments of 25 mV, and from 0 to 100 mV in increments of 20 mV. *C*, internal $[Ca^{2+}]$ was 1.2 μM. Currents were induced by voltage steps to −100 mV and from 0 to 100 mV in increments of 20 mV for WT, and to −180, −50 mV and from 0 to 100 mV in increments of 20 mV for R210N.

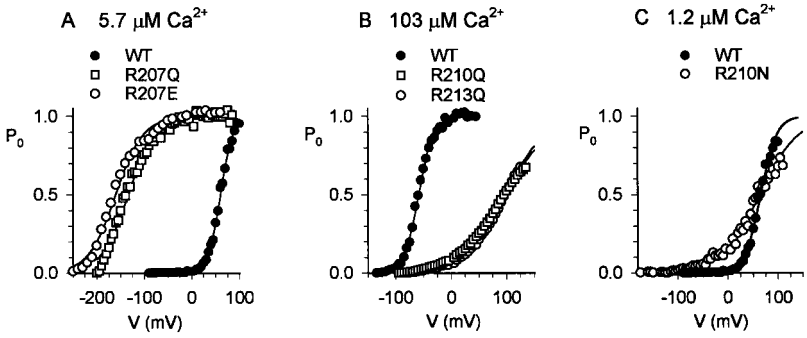

FIG. 3. **Normalized open-state probability (P_O) *versus* voltage curves for WT h*Slo* and S4 mutants.** Data were fitted (solid lines) using the Boltzmann equation (see "Materials and Methods"). *A*, internal Ca^{2+} was 5.7 μM. Values for half-maximum activation, $V_{½}$, and the apparent number of gating charges, z_{eq}, were: 60 mV and 1.9 for WT (*filled circles*), −139 mV and 0.83 for R207Q (*open squares*), and −161 mV and 0.88 for R207E (*open circles*). *B*, internal Ca^{2+} was 103 μM. $V_{½}$ and z_{eq} values were −59 mV and 1.9 for WT (*solid circles*), 96 mV and 0.6 for R210Q (*open squares*), and 98 mV and 0.7 for R213Q (*open circles*). *C*, internal Ca^{2+} was 1.2 μM. $V_{½}$ and z_{eq} values were: 65 mV and 1.5 for WT (*filled circles*) and 63 and 0.65 for R210N (*open circles*).

TABLE I
Parameters describing the voltage dependence of hSlo and S4 mutants

Channel	$V_{½}$[a] (1.7 μM Ca^{2+})	$V_{½}$[a] (10 μM Ca^{2+})	$V_{½}$[a] (103 μM Ca^{2+})	z_{eq}[a]
	mV	*mV*	*mV*	
Wild type	86 ± 17 (36)	12 ± 18 (24)	−18 ± 33 (4)	1.43 ± 0.36 (31)
R201Q		68 ± 26[b] (10)		1.32 ± 0.16 (25)
L204H		11 ± 56 (10)		1.16 ± 0.54 (25)
L204R	92 ± 5 (3)			1.58 ± 0.28 (19)
R207Q	−104 ± 18 (3)			0.73 ± 0.18[b] (45)
R207E		−178 ± 17[b] (9)		0.72 ± 0.15[b] (19)
R210Q			100 ± 38[b] (3)	0.70 ± 0.16[b] (6)
R210N	54 ± 29 (5)			0.50 ± 0.16[b] (7)
R213Q			114 ± 13[b] (4)	0.58 ± 0.08[b] (19)
Q216R	124 ± 41 (2)			1.13 ± 0.25 (9)
E219Q	88 ± 23 (3)			1.26 ± 0.19 (12)
E219K	75 ± 10 (1)			1.51 ± 0.32 (13)
R207Q/ R213Q			141 ± 12[b] (4)	0.51 ± 0.06[b] (20)

[a] Values obtained fitting the P_o-V data to a Boltzmann equation (Equation 1). Values are mean ± S.D.
[b] Values significantly different from WT ($p \leq 0.005$). Numbers in parentheses are number of experiments.

In contrast, in *Shaker* K^+ channel neutralization of lysine 374 or arginine 377 produced nonfunctional channels (22, 23, 35). In h*Slo* these residues correspond to Q216 and E219 (Fig. 1, alignment 2). Most authors have placed glutamate 219 in m*slo* and h*Slo* in the internal S4-S5 linker (6, 8–10, 36). In the alignment of Wallner *et al.* (34), the Glu-219 residue forms part of the S4 segment.

Effects of S4 Point Mutations on the Voltage Activation Curves: Shifts along the Voltage Axis—The effect of five point mutations in the S4 segment on h*Slo* channel activation is depicted in Figs. 2 and 3. In Fig. 2*A*, the [Ca^{2+}] was 5.7 μM and the holding voltage was 0 mV. Both R207Q and R207E mutations induce a clear change in activation kinetics of the h*Slo* channel. In this case currents can be elicited at very negative voltages and all channels are open at −20 mV, a voltage at which less than 10% of the channels are open in the wild type h*Slo* channel (Fig. 3*A*). Fig. 2*B* shows that at 103 μM Ca^{2+}, glutamine substitution for arginines 210 and 213 (R210Q, R213Q) results in channels that could be opened only by applying very positive potentials. At this [Ca^{2+}], mutants R210Q and R213Q have half-activation potentials, $V_{½}$, of 96 and 98 mV, respectively, while the $V_{½}$ for WT channel was –59 mV (Fig. 3*B*). It is of interest to compare the effects of mutations R210Q and R210N on the activation curves. For [Ca^{2+}] = 1.2 μM, $V_{½}$ of the R210N construct was about the same as the one obtained for the wild type channel (Fig. 3*C*). However, the position of the P_o-V curve for the R210N mutant relative to the WT channel is a function of the [Ca^{2+}], and this observation will be discussed in detail below. Summarizing, mutations R207Q and R207E produced leftward shifts along the voltage axis of the P_o-V curve compared with the wild type channel; R210Q and R213Q induced rightward shifts of the P_o-V curve; and mutations L204R, L204H, Q216R, E219Q, and E219K were of minor consequences (Table I).

Number of Gating Charges in Wild Type and Mutant hSlo Channels—Several lines of experimental evidence support the notion that the S4 transmembrane segment in Na^+, Ca^{2+} and K^+ voltage-dependent channels is the voltage sensor (18, 21, 22, 37–40). A prediction of this model is that a reduction in the number of charges in the S4 segment should lead to a reduction in the number of gating charges (z_{eq}; Equation 1) that determine the slope of the Boltzmann distribution around the half activation voltage. Mutations R207Q, R207E, R210N, R210Q, and R213Q decrease the slope of the P_o-V curves (Fig. 3, *A–C*) by 49, 50, 65, 65, 51, and 59%, respectively (Table I). These results support the notion that the S4 basic amino acids are part of the voltage sensor in h*Slo*. By contrast, five mutations of the S4 segment did not significantly alter the slope of the P_o-V curve: L204H, L204R, Q216R, E219Q, and E219K (Table I). Additionally, the neutralization of the arginine 201, which in alignment 2 (34) is located in the S3-S4 linker, did not change the slope of the P_o-V curves (Table I).

The use of a Boltzmann function to fit the P_o-V data assumes a simple two-state model: closed-open. There is compelling evidence that the h*Slo* channel contain several closed and open states (27, 28, 41–46). In this case, a fit to the P_o-V data using Equation 1 may result in an underestimation of the number of gating charges per channel. The total number of gating charges

for channels having an arbitrary number of closed states can be obtained through measurements of gating currents (47). However, h*Slo* gating current measurements require large channel expression and an adequate methodology to measure them, and this has been successfully done only recently (27). Alternatively, a widely used method to obtain the equivalent number of gating charges for a linear model containing any number of closed states is the limiting slope method (LSM) (48). We used LSM to further investigate the mutants for which z_{eq} is lower than that of WT. In order to use the LSM, the $P_o(V)$ data were plotted as $\log(P_o)$ *versus* V (Fig. 4), and the P_o values in the range between 0.001 to 0.01 were fitted to the equation

$$P_o(V) = cte[\exp(z_{eq}limFV/RT)], \qquad \text{(Eq. 2)}$$

where $z_{eq}lim$ is the equivalent number of gating charges at very low P_o. The LSM was applied to the different S4 mutants used in this study, and the results are shown in Fig. 5. The $z_{eq}lim$ was found to be the same as z_{eq} obtained using Equation 1 for the wild type h*Slo* channel. Using the LSM, we could only confirm that neutralization of arginines in positions 210 and 213 were able to significantly reduce the number of gating charges directly coupled to the h*Slo* pore opening (Table I, Fig. 5). The notion that arginine 207 is located outside of the electric field is strengthened by the result obtained with the double mutant R207Q/R213Q. For this mutant, $z_{eq}lim$ was the same as the one found for the single mutant R213Q, suggesting that the neutralization of arginine 207 is unable to reduce the gating charge (Table I).

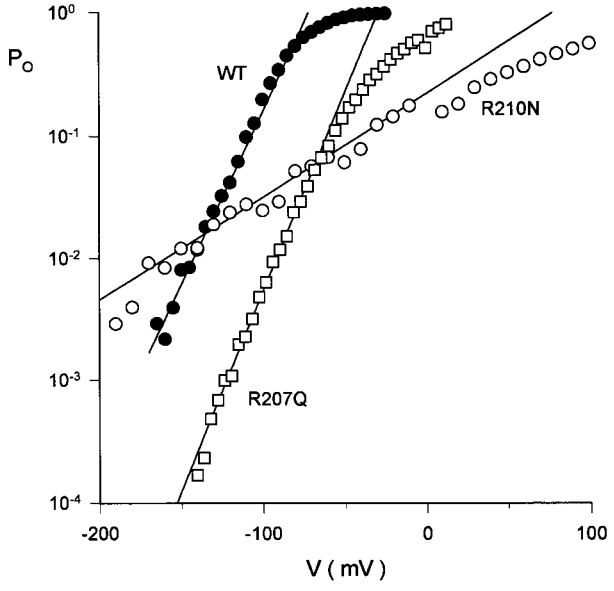

FIG. 4. **$z_{eq}lim$ for WT and S4 mutants.** P_o-V curves as those shown in Fig. 2 were plotted with the ordinate in a logarithmic scale, and fitted with Equation 2, for P_o values ranging between 0.001 and 0.1. $z_{eq}lim$ for WT (*filled circles*), R207Q (*open squares*), and R210N (*open circles*) obtained from linear regression are 1.64, 1.65, and 0.65, respectively. Calcium concentration for WT, R207Q, and R210N were 2.9 mM, 8 pM, and 1 μM, respectively.

Quantitative Description of Results—Cox *et al.* (28) used a voltage-dependent version of the Monod-Wyman-Changeaux model of allosteric proteins considering the MaxiK channel as a homotetramer with a single Ca^{2+} binding site in each subunit. Each subunit can be in a reluctant (R) or in a permissive (P) state, and only those channels containing the four subunits in the P configuration are conductive. For each subunit, we have the scheme below.

$$\begin{array}{ccccc} & & K_c & & \\ & R & \rightleftarrows & R\text{-}Ca & \\ K_1(V) & \Updownarrow & & \Updownarrow & K_2(V) \\ & P & \rightleftarrows & P\text{-}Ca & \\ & & K_o & & \end{array}$$

SCHEME I

$K_1(V)$ and $K_2(V)$ are the voltage-dependent equilibrium constants connecting R and P states with and without Ca^{2+} bound, respectively, and K_c and K_o are the dissociation constants for Ca^{2+} from the R and P configurations, respectively.

In the present study, we used the model of Cox *et al.* (28) in which four Ca^{2+} ions bind to the channel and the microscopic dissociation constants depend only on whether the subunit is in the R or P configurations. This model is sufficient to give a good fit to the data obtained with the wild type h*Slo* and to interpret the S4 mutant results mechanistically. The model predicts that the probability of opening is given by the relation (28)

$$P_o = 1/\{1 + [(1 + [Ca]/K_c)/(1 + [Ca]/K_o)]^4 K_1(V)\}, \qquad \text{(Eq. 3)}$$

where $K_1(V) = \exp[(\Delta G_0 - z_{eq}FV)/RT]$ and ΔG_o is the free energy difference between the open and closed configuration of the h*Slo* channel at $V = 0$ and $[Ca^{2+}] = 0$.

From Equation 3, we find that the voltage at which $P_o = 0.5$, $V_{1/2}$, is:

$$V_{1/2} = (\Delta G_o + RT \ln B)/(zF), \qquad \text{(Eq. 4)}$$

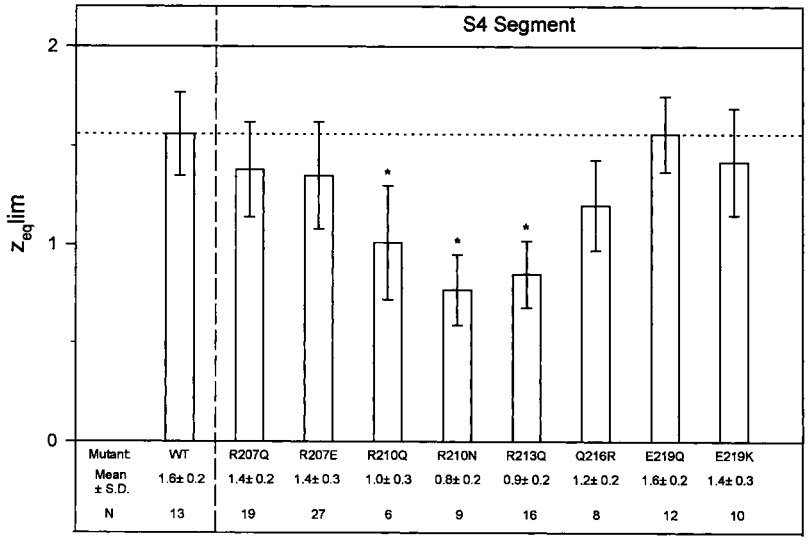

FIG. 5. **Number of apparent gating charges for wild type and S4 mutants h*Slo* channels.** The number of equivalent gating charges ($z_{eq}lim$) was obtained fitting an exponential function to the P_o-V curves for values of P_o lower than 0.1. Average, standard deviation (S.D.), and number of determinations are indicated for each channel. *, values significantly different to WT ($p \leq 0.005$).

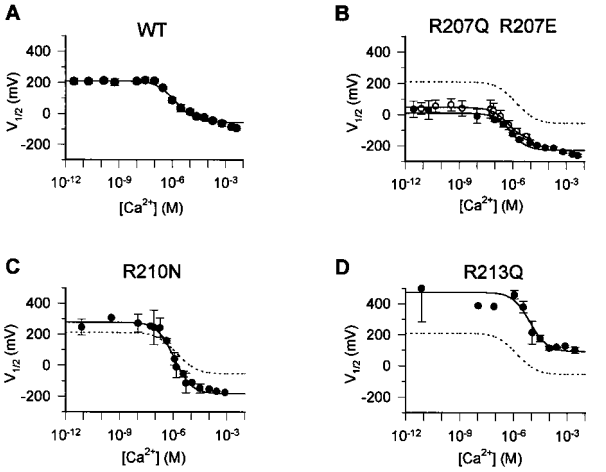

FIG. 6. *A*, $V_{½}$ *versus* [Ca^{2+}] relationship for wild type h*Slo*. $V_{½}$ values were obtained from the fit of a Boltzmann distribution to the normalized conductance *versus* voltage curves (P_o-V curves), and were plotted against the corresponding [Ca^{2+}]. The *solid line* is the fitting with Equation 4 to the data. Fitting parameters are given in Table II. *B*, the $V_{½}$ for WT h*Slo* is plotted as a *broken line* along the corresponding values for the S4 mutants R207Q (*open circles*) and R207E (*solid circles*) that were fitted using Equation 4 (*solid lines*). *C*, same as in *B* but for the R210N. mutant. Data (*solid circles*) were fitted using Equation 4 (*solid line*). *D*, same as in *C* but for the R213Q mutant.

where $B = [(1 + [Ca]/K_c)/(1 + [Ca]/K_o)]^4$. Notice that when $[Ca^{2+}] \gg K_c$ and K_o, $B = (K_o/K_c)^4$ and when $[Ca^{2+}] \to 0$, $B = 1$, hence

$$\Delta G_o = z_{eq} F V_{½(Ca=0)} \qquad \text{(Eq. 5)}$$

and

$$V_{½(Ca=0)} - V_{½(Ca=\infty)} = (4RT/z_{eq}F)\, ln(K_o/K_o). \qquad \text{(Eq. 6)}$$

The change in conformational energy difference between open and closed configuration of the channel induced by Ca^{2+} binding, *A*, is given by the following equation.

$$A = z_{eq} F[V_{½(Ca=0)} - V_{½(Ca=\infty)}] \qquad \text{(Eq. 7)}$$

The parameter *A* can be viewed as a measure of the coupling between Ca^{2+} binding and pore opening. *A* is calculated from the ratio K_c/K_o, which can be obtained fitting the $V_{½}$-[Ca^{2+}] data using Equation 4. Fig. 6*A* shows that a fit to the WT h*Slo* data using Equation 4 is reasonably good in the range of [Ca^{2+}] between 10^{-12} to 10^{-4} M (*cf.* Ref. 28). Notice that, below 10^{-7} M Ca^{2+}, both the model and the experimental results show that $V_{½}$ is [Ca^{2+}]-independent. This Ca^{2+}-independent behavior has been observed previously (26, 27, 49) in WT h*Slo* channels but has been questioned because of uncertainties on G_{max} determination (49). Our results on R207Q and R207 mutants are not subject to the same criticism since they can reach their maximal P_o even at very low [Ca^{2+}]. We found that, in the mutants R207Q and R207E, $V_{½}$ is constant at $[Ca^{2+}] \leq 10^{-7}$ M, a range where $V_{½}$ is approximately +30 mV (Fig. 7*A*). These observations further support the notion that the h*Slo* channel is intrinsically voltage-dependent.

As stated before, mutations R207Q, R207E, R210Q, and R213Q in the S4 domain of h*Slo* produced pronounced shifts of the voltage activation curve along the voltage axis (Fig. 3 and Table I). Specifically, mutations R207Q and R207E shift the P_o-V curves by about 150 mV to the left along the voltage axis. In the $V_{½}$-[Ca^{2+}] plane, the curves for these mutants are displaced downward and are essentially parallel to that obtained for the wild type channel (Fig. 6*B*). A fit to the data using Equation 4 indicates that mutants R207Q and R207E mainly

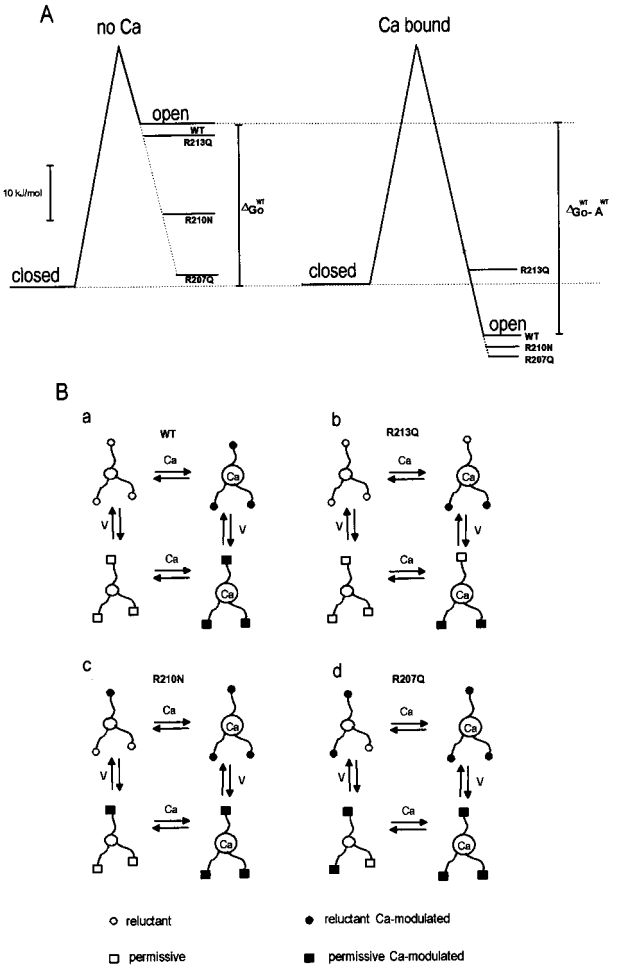

FIG. 7. *A*, schematic representation of the free energies of the open and closed configurations of the WT h*Slo* and S4 mutants in the absence and in the presence of a saturating internal [Ca^{2+}]. Energy at the peak is arbitrary. *Ba,* schematic representing a WT h*Slo* channel subunit in its four possible configurations. The subunit contains three gating particles that can be in the reluctant (*circles*) or in the permissive (*squares*) configurations. Voltage induces the configurational change from reluctant to permissive to in a single step. Calcium binding decreases the energy to perform the change from the reluctant to the permissive configuration (*solid symbols*) mediated by voltage. *Bb,* in the R213Q mutant, one of the gating particles was uncoupled to the calcium binding. In this case, if *a* is the free energy necessary to induce the configurational change of one gating particle, the channel subunit in the absence of Ca^{2+} behaves very similarly to the WT h*Slo* subunit. However, it takes *a* kJ/mol more to change the subunit from the reluctant to the permissive configuration in the presence of Ca^2. *Bc*, in the R210N mutant one of the gating particles was uncoupled to the calcium binding but has the configuration of a Ca-bound gate (*solid symbols*). Therefore, in this case it takes *a* kJ/mol less energy to displace the equilibrium from the reluctant to the permissive forms in the absence of Ca^{2+}. The Ca^{2+}-bound subunit behaves like the WT h*Slo* subunit. *Bd*, the R207Q channel subunit has two gates uncoupled to Ca binding as in R210N. In this case, it takes 2*a* less energy to induce the change from the reluctant to the permissive form in the absence of Ca^{2+}. The Ca^{2+}-bound subunit behaves like the WT h*Slo* subunit.

decrease ΔG_o compared with the WT channel (Table II; Fig. 7*A*). These mutations also induced a reduction in parameter *A* (Table II; Fig. 7*A*). For the R210N mutant, the $V_{½}$ is 50 mV higher than the WT channel at [Ca^{2+}] below 10^{-7} M (Fig. 7*B*). Due to the smaller z_{eq} of the R210N mutant, a crossover of the mutant and the WT channel $V_{½}$-[Ca^{2+}] curves occurs at about 1 μM Ca^{2+} (Fig. 6*C*). The parameter *A* also decreases in this mutant (Table II; Fig. 7*A*). Mutations R210Q and R213Q (Fig. 3*B*, Table I) decrease z_{eq} and shifted the activation curves to very positive potentials at all [Ca^{2+}] tested (Fig. 6*D*). The shift

in $V_{½}$ at $[Ca^{2+}] < 10^{-7}$ M is fully accounted for by a change in z_{eq} since ΔG_o does not change with respect to the WT h*Slo* (Table II, Fig. 7*A*). We expect a crossover of the mutant and wild type $V_{½}$-$[Ca^{2+}]$ curves if the effect of the mutation is a change in z_{eq} only (*cf.* Fig. 6*C*). This crossover does not occur in this mutant due to a decrease in the coupling parameter *A* (Table II; Fig. 7*A*). We do not have enough data to interpret the effects of the R210Q mutant in terms of the model.

DISCUSSION

Voltage-sensing Residues in the S4 Segment of hSlo and Shaker K^+ Channels—The results shown in this work demonstrate that the S4 segment of the MaxiK h*Slo* is an important part of the voltage sensor of the channel. In contrast to voltage-gated K^+ channels (K_V) h*Slo* seems to have only three positive residues in its S4 segment: the arginines in positions 207, 210, and 213 (Fig. 1, alignment 2). The neutralization of these residues decreases the slope of the *G-V* curves and shifts the curves in the voltage axis, suggesting that these residues are part of the voltage sensor. However, if the number of equivalent gating charges is determined by the limiting slope method, we found that only arginines in positions 210 and 213 contribute significantly to the number of charges per channel. In the voltage-dependent K^+ channel, *Shaker*, the equivalent residues in the S4 segment are also arginines: Arg-365, Arg-368, and Arg-371 (Fig. 1). These three basic residues in the S4 segment contribute significantly to the gating charge (24). On the other hand, Aggarwal and MacKinnon (17) have counted wild type and S4 mutant *Shaker* channels using radiolabeled agitoxin, a high affinity blocker, and measured the total gating charge in each case. They found that only residues Arg-362, Arg-365, Arg-368, and Arg-371 sense the transmembrane voltage. It is surprising, therefore, that although h*Slo* possesses three equivalent positively charged residues out of the four that are responsible for the voltage dependence in *Shaker*, the voltage dependence of h*Slo* is much smaller (see below and Table I). One possible explanation for the smaller number of gating charges in h*Slo* is that residue Arg-207 in h*Slo* appears not to contribute significantly to the total charge per channel. The residue equivalent to Arg-207 in *Shaker* K^+ channels, Arg-365 (Fig. 1, alignment 2), contributes with five electronic charges.[2] Moreover, in *Shaker* K^+ channels, residue Glu-293 in S2 also constitutes a significant part of the voltage sensor (24, 35, 50). The mutation E293Q in *Shaker* reduced the charge per channel from 13 e_o to 7 e_o. According to Wallner *et al.* (34) alignment, for h*Slo* and *dSlo* S2 region, the residue Glu-293 in *Shaker* is not conserved in these channels, but a tyrosine (Tyr-163) is present. The lack of this important negative charge in MaxiK channels may also contribute to their weaker voltage dependence. It is also important to note here that Papazian *et al.* (35) proposed, on the basis of rescue experiments with double mutations, that in *Shaker* K^+ channels Lys-374 might form a charge network with Glu-293 in S2 and Asp-316 in S3. In *Shaker*, the mutant channel K374Q is not functional and is rescued by either neutralizing Glu-293 to a Gln (equivalent to Tyr-163 in h*Slo*) or Asp-316 to Asn (35). In h*Slo*, in the equivalent position to Lys-374, there is a glutamine at 216 (Fig. 1, alignment 2). It is tempting to suggest following the analogy between these two K^+ channels, that h*Slo,* despite the fact it contains a glutamine in position 216, matures properly because there is a neutral residue, a tyrosine, in position 163.

[2] Notice, that in the case of neutralization of residue 365 in *Shaker* leads to an unexpected result, since we expect that R365 should contribute no more than four charges, *i.e.* if one charge per subunit is eliminated, four charges per channel are eliminated only if they move through the entire electric field. As pointed out by Seoh *et al.* (24), this result can be explained if the neutralization induces a voltage drop that occurs over a large extent of the protein. This implies that the results of charge neutralizations should be taken cautiously. However, the results of Larsson *et al.* (18) and Seoh *et al.* (24) are strong evidence that, upon channel activation, there is a displacement of residues Arg-365, Arg-368, and Arg-371 in *Shaker* K^+ channels and that these residues contribute to the total charge per channel.

TABLE II

Gating model parameters for wild type and S4 mutant hSlo channels

Parameters ΔG_o, K_c, and K_o were obtained from the fitting of Equation 4 to the $V_{½}$-$[Ca^{2+}]$ relationships shown in Fig. 6, using the z_{eq} values from Table I. A was calculated from K_c/K_o ratio using equations 9 and 10. Since K_c and K_d are correlated, the error of *A* was obtained rerunning the curve fitting using ΔG_o, K_o, and K_c/K_o ratio as adjustable parameters. Errors given were read from the diagonal elements of the final error matrix of the least square fitting procedure.

Channel	ΔG_o	K_c	K_o	*A*
	kJ/mol	*μM*	*μM*	*kJ/mol*
WT	29 ± 5	10.0 ± 2.1	0.20 ± 0.06	38 ± 2
R201Q	30 ± 2	14.7 ± 7.1	0.61 ± 0.31	29 ± 3
L204H	21 ± 3	20.3 ± 4.4	1.03 ± 0.19	31 ± 1
R207Q	3 ± 2	1.2 ± 0.2	0.30 ± 0.04	16 ± 1
R207E	1 ± 6	1.8 ± 0.5	0.30 ± 0.09	18 ± 1
R210N	13 ± 5	3.5 ± 0.6	0.40 ± 0.05	24 ± 1
R213Q	27 ± 13	25.1 ± 8.5	2.90 ± 1.25	24 ± 2
E219K	29 ± 6	14.9 ± 5.2	0.40 ± 0.18	38 ± 2

Energy Diagrams for the Wild Type and S4 Mutant Channels: A Pictorial Representation—Fig. 7*A* shows the free energy diagrams of the channel in the absence of and after Ca^{2+} binding at zero applied voltage taking the closed state as a reference. In the absence of Ca^{2+}, we need to supply the h*Slo* WT type channel with 29 kJ/mol in order to reach a $P_o = 0.5$. This energy is about the same for the R213Q mutant but it is less for the R210N, becoming negligible for the R207Q mutant. When the channel binds Ca^{2+}, the free energy of the open configuration is below that of the closed state and channels are mostly open at zero voltage. Similar energies for the open configuration are found for the R210N and R207Q mutants. For the R213Q mutant, the effect of Ca^{2+} binding on the open configuration is not enough to displace the equilibrium toward the open state. The energy difference associated with Ca^{2+} binding is smaller for all mutants compared with the h*Slo* WT channel.

In order to have a pictorial view of the changes in channel conformation introduced by the mutations, we fancy each channel subunit as shown in Fig. 7*B*. In the allosteric model of Cox *et al.* (28), the voltage sensor from each subunit moves in a highly concerted way such that their movement is represented by a single voltage dependent step. Consider for the sake of illustration a single channel subunit that is in the reluctant state with a voltage sensor consisting of three gating particles represented in Fig. 7*B* (*a*) as open circles. The simultaneous displacement of the particles induced by the applied voltage modifies the subunit conformation from the reluctant to the permissive state. For a channel to open, it is necessary that the four subunits reach the permissive state. The voltage-dependent conformational change is represented in Fig. 7*B* (*a*) with a change in the gating particle shape from open circles to squares (permissive). The free energy associated with the displacement of one particle, δg, is modulated by Ca^{2+} in such a way that if the subunit binds Ca^{2+}, δg is decreased by an amount *a*. In other words, binding of Ca^{2+} decreases the energy difference between the reluctant (*closed circles*) and the permissive (*closed squares*) states of the subunit by 3*a*. In the mutant R213Q, the equilibrium between reluctant and permissive forms of the subunit in the absence of Ca^{2+} is unchanged with respect to the WT h*Slo* channel (Fig. 7*B*, *b*). However, one of the particles of the voltage sensor of this particular mutant fails to be modulated by Ca^{2+} (*right side* of Fig. 7*B*, *b*). In this case,

Ca^{2+} binding to the channel subunit is less effective in modulating the configuration of the voltage sensor (*i.e.* energy decreases by only 2*a*). On the other hand, in the mutant R210N, one of the gating particles has the Ca^{2+}-modulated conformation even if no Ca^{2+} is bound to the subunit (Fig. 7*B*, *c*). In this case, the energy supplied by the electric field needed to induce the conformational change that leads to the permissive subunit state is *a* kJ/mol smaller than in the case of the WT channel. Binding of Ca^{2+} to the subunit modulates the remaining two gating particles, and the resulting structure behaves similarly to the WT channel. Fig. 7*B* (*d*) shows that in the absence of Ca^{2+} two of the gating particles of the R207Q mutant are in the Ca^{2+}-modulated conformation. The conformation of the voltage sensor of the R207Q mutant is such that the channel subunit is in the permissive conformation even in the absence of an applied voltage. The R207Q mutant behaves like the wild type subunit when it binds Ca^{2+} (*right side* of Fig. 7*B*, *d*).

Model Adequacy—As discussed recently by Rothberg and Magleby (44), the MWC model we have used in the present study could approximate the basic features of the Ca^{2+} dependence of the kinetic structure. Cox *et al.* (28) found that the MWC model gives an adequate description for the effects of voltage and Ca^{2+} on P_o for m*Slo* channels. We think this model is appropriate to account for the data obtained with the WT and the S4 mutants described in the present study. Furthermore, it provided a heuristic device to interpret the data in terms of thermodynamic parameters. However, it is clear that more complex models need to be used when trying to give a detailed description of the channel voltage-dependent gating kinetics (27, 44, 46). In this regard, the MWC model fails to predict the observed Cole-Moore shift, the charge movement between open states (27), and to account for the brief closed intervals (44).

Our results suggest that the S4 segment in the h*Slo* channel plays the role of the voltage sensor and that Ca^{2+} acts by decreasing the intrinsic configurational energy difference that separates the closed from the open state at zero applied voltage. This conclusion is further supported by the observation that for the wild type h*Slo* channel the same amount of gating charge is moved in the Ca^{2+}-dependent and in the Ca^{2+}-independent activation regions (27).

Acknowledgment—We thank E. Rosenman for excellent technical assistance.

REFERENCES

1. Toro, L., Wallner, M., Meera, P., Tanaka, Y. (1998) *News Physiol. Sci.* **13,** 112–117
2. Vergara, C., Latorre, R., Marrion, N. V., Adelman, J. P. (1988) *Curr. Opin. Neurobiol.* **3,** 321–329
3. Jan, L. Y., and Jan, Y. N. (1990) *Nature* **345,** 672
4. Atkinson, N. S., Robertson, G. A., and Ganetzky, B. (1991) *Science* **253,** 551–555
5. Adelman, J. P., Shen, K. Z., Kavanaugh, M. P., Warren, R. A., Wu, Y. N., Lagrutta, A., Bond, C. T., and North, R. A. (1992) *Neuron* **9,** 209–216
6. Butler, A., Tsunoda, S., McCobb, D. P., Wei, A., and Salkoff, L. (1993) *Science* **261,** 221–224
7. Dworetzky, S. I., Trojnacki, J. T., and Gribkoff, V. K. (1994) *Mol. Brain Res.* **27,** 189–193
8. McCobb, D. P., Fowler, N. L., Featherstone, T., Lingle, C. J., Saito, M. Krause, J. E., and. Salkoff, L. (1995) *Am. J. Physiol.* **269,** H767–H777
9. Pallanck, L., and Ganetzky, B. (1994) *Hum. Mol. Genet.* **3,** 1239–1243
10. Tseng-Crank, J., Foster, C. D., Krause, J. D., Mertz, R., Godinot, N., DiChiara, T. J., and Reinhart, P. H. (1994) *Neuron* **13,** 1315–1330
11. Wallner, M., Meera, P., Ottolia, M., Kaczorowski, G., Latorre, R., Garcia, M. L., Stefani, E., and Toro, L. (1995) *Receptors Channels* **3,** 185–199
12. Wei, A., Jegla, T., and Salkoff, L. (1996) *Neuropharmacology* **35,** 805–829
13. Jiang, G. J., Zidanic, M., Michaels, R. L., Michael, T. H., Griguer, C., and Fuchs, P. A. (1997) *Proc. R. Soc. Lond. B Biol. Sci.* **264,** 731–737
14. Catterall, W. A. (1986) *Annu. Rev. Biochem.* **55,** 953–985
15. Guy, H. R., and Seetharamulu, P. (1986) *Proc. Natl. Acad. Sci. U. S. A.* **83,** 508–512
16. Noda, M., Shimizu, S., Tanabe, T., Takai, T., Kayano, T., Ikeda, T., Takahashi, H., Nakayama, H., Kanaoka, Y., Minamino, N., Kanagawa, K., Matsuo, H., Raftery, M. A., Hirose, T., Inayama, S., Hayashida, H., Miyata, T., and Numa, S. (1984) *Nature* **312,** 121–127
17. Aggarwal, S. K., and MacKinnon, R. (1996) *Neuron* **16,** 1169–1177
18. Larsson, H. P., Baker, O. S., Dhillon, D. S., and Isacoff, E. Y. (1996) *Neuron* **16,** 387–397
19. Liman, E. R., Hess, P., Weaver, F., and Koren, G. (1991) *Nature* **353,** 752–756
20. Logothetis, D. E., Movahedi, S. Satler, C. Lindpaintner, K., and Nadal-Ginard, B. (1992) *Neuron* **3,** 531–540
21. Mannuzzu, L. M., Moronne, M. M., and Isacoff, E. Y. (1996) *Science* **271,** 213–216
22. Papazian, D. M., Timpe, L. C., Jan, Y. N., and Jan, L. Y. (1991) *Nature* **349,** 305–310
23. Perozo, E., Santacruz-Toloza, L., Stefani, E., Bezanilla, F., and Papazian, D. (1994) *Biophys. J.* **66,** 345–354
24. Seoh, S.-A., Sigg, D., Papazian, D., and Bezanilla, F. (1996) *Neuron* **16,** 1159–1167
25. Starace, D., Stefani, E., and Bezanilla, F. (1997) *Neuron* **19,** 1319–1327
26. Meera, P., Wallner, M., Jiang, Z., and Toro, L. (1996) *FEBS Lett.* **382,** 84–88
27. Stefani, E., Ottolia, M., Noceti, F., Olcese, R., Wallner, M., Latorre, R., and Toro, L. (1997) *Proc. Natl. Acad. Sci. U. S. A.* **94,** 5427–5431
28. Cox, D. H., Cui, J., and Aldrich, R. W. (1997a) *J. Gen. Physiol.* **110,** 257–281
29. Horton, R. M., Hunt, H. D., Ho. S. N., Pullen, J. K., and Pease, L. R. (1989) *Gene* (*Amst.*) **77,** 61–68
30. Landt, O., Grunert, H.-P., and Hahn, U. (1990) *Gene* (*Amst.*) **96,** 125–128
31. Schoenmakers, T. J., Visser, G. J., Flik, G., and Theuvenet, A. P. R. (1992) *BioTechniques* **12,** 870–874
32. Oberhauser, A., Alvarez, O., and Latorre, R. (1988) *J. Gen. Physiol.* **92,** 67–86
33. Cox, D. H., Cui, J., and Aldrich, R. W. (1997b) *J. Gen. Physiol.* **109,** 633–646
34. Wallner, M., Meera, P., and Toro, L. (1996) *Proc. Natl. Acad. Sci. U. S. A.* **93,** 14922–14927
35. Papazian, D. M., Shao, X. M., Seoh, S-A., Mock, A. F., Huang, Y., and Wainstock, D. H. (1995) *Neuron* **14,** 1293–1301
36. Wei, A., Solaro, C. R., Lingle, C. J., and Salkoff, L. (1994) *Neuron* **13,** 671–681
37. Stühmer, W., Conti, F., Suzuki, H., Wang, X., Noda, M., Yahagi, N., Kubo, H., and Numa, S. (1989) *Nature* **339,** 597–603
38. Yang, N., and Horn, R. (1995) *Neuron* **15,** 213–218
39. Yang, N., George, A. L. J., and Horn, R. (1996) *Neuron* **16,** 113–122
40. García, J., Nakai, J., Imoto, K., and Beam, K. G. (1996) *Biophys. J.* **72,** 2515–2523
41. DiChiara, T. J., and Reinhart, P. H. (1995) *J. Physiol.* **489,** 403–418
42. McManus, O. B., and Magleby K. L. (1991) *J. Physiol.* **443,** 739–777
43. Moczydlowski, E., and Latorre, R. (1983) *J. Gen. Physiol.* **82,** 511–542
44. Rothberg, B. S., and Magleby, K. L. (1998) *J. Gen. Physiol.* **111,** 751–780
45. Silberberg, S. D., Lagrutta, A., Adelman, J. P., and Magleby, K. L. (1996) *Biophys. J.* **70,** 2640–2651
46. Wu, Y. C., Art, J. J., Goodman, M. B., and Fettiplace, R. (1995) *Prog. Biophys. Mol. Biol.* **63,** 131–158
47. Schoppa, N. E., McCormack, K., Tanouye, M. A., and Sigworth, F. J. (1992) *Science* **255,** 1712–1715
48. Almers, W. (1978) *Rev. Physiol. Biochem. Pharmacol.* **82,** 96–190
49. Cui, J., Cox, D. H., and Aldrich, R. W. (1997) *J. Gen. Physiol.* **109,** 647–673
50. Planells-Cases, R., Ferrer-Montiel, V., Patten, C. D., and Montal, M. (1995) *Proc. Natl. Acad. Sci. U. S. A.* **92,** 9422–9426